PERIODICA POLYTECHNICA SER. MECH. ENG. VOL. 45, NO. 2, PP. 217–237 (2001)

INCORPORATION OF FORWARD BLADE SWEEP IN THE NON-FREE VORTEX DESIGN METHOD OF AXIAL FLOW TURBOMACHINERY ROTORS

János VAD

Department of Fluid Mechanics
Budapest University of Technology and Economics
H–1111 Budapest, Bertalan Lajos u. 4–6., Hungary
Tel.: (+36-1) 463 2464, 463 4072
Fax: (+36-1) 463 3464
e-mail: vad@simba.ara.bme.hu

Received: 8 January, 2001

Abstract

The paper presents a novel strategy for design of high-performance non-free vortex axial flow rotors with forward swept blades. The design methodology incorporates the determination of an optimum extent of forward blade sweep into the non-free vortex design methodology, considering the realistic three-dimensional blade-to-blade flow. The design methodology is to be completed with Computational Fluid Dynamics analysis and global measurements on the turbomachinery unit. A fan rotor design example is presented.

Keywords: axial flow turbomachinery, non-free vortex design, blade sweep, computational fluid dynamics, characteristic curve and efficiency measurements.

1. Introduction

Sweeping forward the blades of axial flow turbomachinery rotors offers a potential for improvement of operational characteristics of the turbomachinery unit. In the past years, a number of Computational Fluid Dynamics (CFD) investigations and experiments pointed out advantageous tendencies related to forward blade sweep. Measurements by MOHAMMAD and RAJ [17], WRIGHT and SIMMONS [30], and YAMAGUCHI et al. [31] as well as experiments and CFD studies by BEILER [2] and discussion by BREUGELMANS [4] confirmed that stage performance and efficiency can be improved by sweeping the blades forward in an appropriate manner. The above authors dedicated these favourable tendencies mostly to suppression of secondary losses in the blade passages and in the blade tip region. WENNERSTROM and PUTERBAUGH [29] and LAKSHMINARAYANA [15] conclude that by sweeping the blades, onset of compressibility and the related shock losses can be reduced. WRIGHT and SIMMONS [30], KODAMA and NAMBA [13], and SRIVASTAVA and MEHMED [19] establish that the noise generated by the turbomachinery unit can also be reduced by forward blade sweep. Although forward sweep raises blade mechanical problems, such difficulties can be eliminated by use of appropriate rotor

blade materials (SRIVASTAVA and MEHMED [19]; THOMSON et al. [20]).

It is acknowledged that the simultaneous application of sweep and dihedral, which may even change along the radius as appropriate, offers a unique possibility for fluid dynamic improvement of blading. However, such special prescription of blade stacking line introduces difficulties in blade design. Systematic design optimisation of blade sweep is a great challenge due to the complexity of rotor interblade flow and difficulties in judgement of sweep effects on blade aerodynamics. Harmonisation of swept blade geometry and 3D blade-to-blade flow is in lack of generally applicable concepts. The optimum measure and manner of sweeping the blades is sought even in some recent research programs by means of testing various rotors of blade sweep prescribed in an arbitrary manner (e.g. GLAS and KUHN [9]; BEILER and CAROLUS [2]; GLAS [10]; KUHN [14]).

The overview of technical literature suggests the author to conclude that favourable effects of forward sweep have been pointed out often in cases when a spanwise gradient of blade circulation was present in the rotor. In such studies, the rotor blade circulation was increasing with radius either due to the non-free vortex (NFV) design concept (e.g. VAD and BENCZE [21]) or/and due to part load (flow rate lower than design). MOHAMMAD and RAJ [17] found improved performance characteristics due to forward sweep in the part load operational range. WRIGHT and SIMMONS [30] reported that forward sweep resulted in increased total pressure rise peak, shift of stall margin towards lower flow rate, and increased pressure rise together with improved characteristics of boundary layer flow in the part load range. The compressor rotor studied by YAMAGUCHI et al. [31] was designed for NFV operation. YAMAGUCHI et al. [31] observed that sweeping the compressor rotor blades forward led to an increased efficiency, and to a more accurate realization of design radial distribution of flow coefficient and relative outflow angle. The research program carried out on swept blades by BEILER [1] and BEILER and CAROLUS [2] regarded also rotors of NFV design, giving a further confirmation of advantages of sweep. For a rotor in which a slight blade circulation gradient is present (FV design rotor in VAD et al. [27]), GLAS [9] predicted that optimum fluid dynamic characteristics and increased efficiency can be achieved if the blades are swept slightly forward. This tendency is also confirmed with study of works by GLAS [10] and KUHN [14].

On the basis of above, it is expected that the advantages of forward sweep can be mostly utilized for blades designed for NFV operation. The NFV rotor blading of appropriate forward sweep can accommodate the three-dimensional (3D) interblade flow corresponding to shed vorticity due to NFV operation, thus resulting in improved fluid dynamical characteristics. The NFV design method, i.e. spanwise increasing prescribed rotor blade circulation, is widely used for design of high performance turbomachines (e.g. LAKSHMINARAYANA [15]). For this reason, it is of great practical importance to find an appropriate concept for incorporation of forward blade sweep in NFV design.

This paper draws guidelines to a novel NFV design method incorporating the forward sweep of blades systematically in fluid dynamic blade optimisation. The application of the design methodology is illustrated in a fan rotor design example.

2. Background and Test Rotor

Department of Fluid Mechanics, Budapest University of Technology and Economics maintains an active research program on high performance axial flow fans of NFV design. Several fan units of unswept blades have been designed and tested through global (characteristic curve and efficiency) measurements. Details of the flow fields developing upstream and downstream of selected rotors were measured using Laser Doppler Anemometry (LDA). Thanks to a significant contribution of Department of Mechanics and Aeronautics, University of Rome 'La Sapienza' to the research program, the means of turbomachinery research have been supplemented with a powerful CFD tool called 'XENIOS'. This CFD technique offers a unique possibility for investigation of interblade flow phenomena, which were not accessible for the LDA tool.

One unswept rotor of which flow characteristics were found especially favourable (designated 'BUP-29' in VAD and BENCZE [21]) was investigated by means of a concerted application of LDA and CFD techniques in Hungarian – Italian cooperation (CORSINI et al. [6]; VAD et al. [23]). In further collaborative studies on the same rotor, design aspects of blade sweep in NFV design have been outlined (VAD et al. [24]; VAD et al. [26]).

The design example given in this paper regards a high performance model rotor of forward swept blades, designated hereby as SWUP-35 and to be studied by means of CFD in a following common paper (CORSINI et al. [7]). Such studies are harmonized with the collaborative research carried out so far. This means that the basic geometrical and design flow parameters of the formerly studied unswept bladed rotor (BUP-29) and the presently discussed swept bladed rotor must be identical. As a consequence, a reasonable comparison can be carried out between the unswept (BUP-29) and swept rotors in order to explore the effects of blade sweep on rotor fluid dynamics. According to the above, and referring to former papers reporting the characteristics of the unswept rotor (VAD and BENCZE [21], [22]; CORSINI et al. [6]), the global geometrical characteristics of the high performance swept bladed NFV rotor in the design example are as follows: ducted isolated axial flow rotor, blade number $N = 12$, casing radius $r_c = 0.315$ m, average tip clearance $\tau = 0.002$ m, hub-to-casing diameter ratio $\nu = 0.676$. The design global flow coefficient is $\Phi = 0.50$ and the design global ideal total pressure rise coefficient is $\Psi = 0.7$. It is expected from the rotor to carry out a rotor efficiency of $\overline{\eta} = 0.88$. The rotor is built up from blades of circular arc camber lines, with a thin profile of uniform thickness along the camber lines, rounded at the leading and trailing edges.

3. Outline of Blade Design Strategy

The presently proposed computer-aided design strategy of forward swept NFV axial flow rotors is outlined in *Fig. 1*. The design methodology incorporates the following

items:

A. The global operational parameters of the turbomachinery unit (flow coefficient, total pressure rise coefficient, efficiency) reflecting the application demands must be established.

B. The basic geometrical data of the rotor (hub-to-casing ratio, blade number, tip clearance) must be selected in accordance with the global operational parameters, on the basis of general design guidelines. The rotor inlet flow condition must be prescribed on the basis of upstream flow measurements or auxiliary CFD data. (The inlet condition includes swirl at the presence of inlet guide vane.) A preliminary NFV outlet swirl function must also be prescribed appropriately in the present design step, according to design experiences.

C. A rotationally symmetric, quasi-3D theoretical rotor flow field must be computed using basic fluid dynamical considerations, in accordance with the global operational parameters. The rotationally symmetric flow solution and a preliminary unswept blade design approach procedure are mutually coupled in an iterative manner the following way. An approximate knowledge of blade geometry is necessary for estimation of spanwise loss and radial velocity distribution playing role in the rotationally symmetric flow solution. On the other hand, the knowledge of rotationally symmetric theoretical flow is essential for preliminary calculation of blade geometry.

D. A CFD study must be carried out on the rotor flow of preliminary unswept blading.

E. The 3D blade-to-blade flow must be modelled. After pitchwise averaging, the blade-to-blade flow model must correspond to the rotationally symmetric theoretical flow solution at inlet and outlet. The torsion of stream surface segments inside the blading, i.e. inclination of streamlines in the blade passages is estimated on the basis of the CFD study.

F. A swept blade design must be carried out, resulting in optimum blade geometrical parameters. An optimum extent of forward sweep is determined ensuring a harmonization of blade passage geometry with the 3D blade-to-blade flow.

G. The swept blade geometry must be tested through concerted CFD studies and experiments (characteristic curve and efficiency measurements).

H. If the application demands are fulfilled, the design procedure is completed. If not, a modification of theoretical flow field and a 3D blade-to-blade flow model must be carried out on the basis of a parallel consideration of CFD and global experimental data. The swept blade design, the CFD study and the experimental verification must be carried out in an iterative manner.

In the following chapters, details of the design phases are presented.

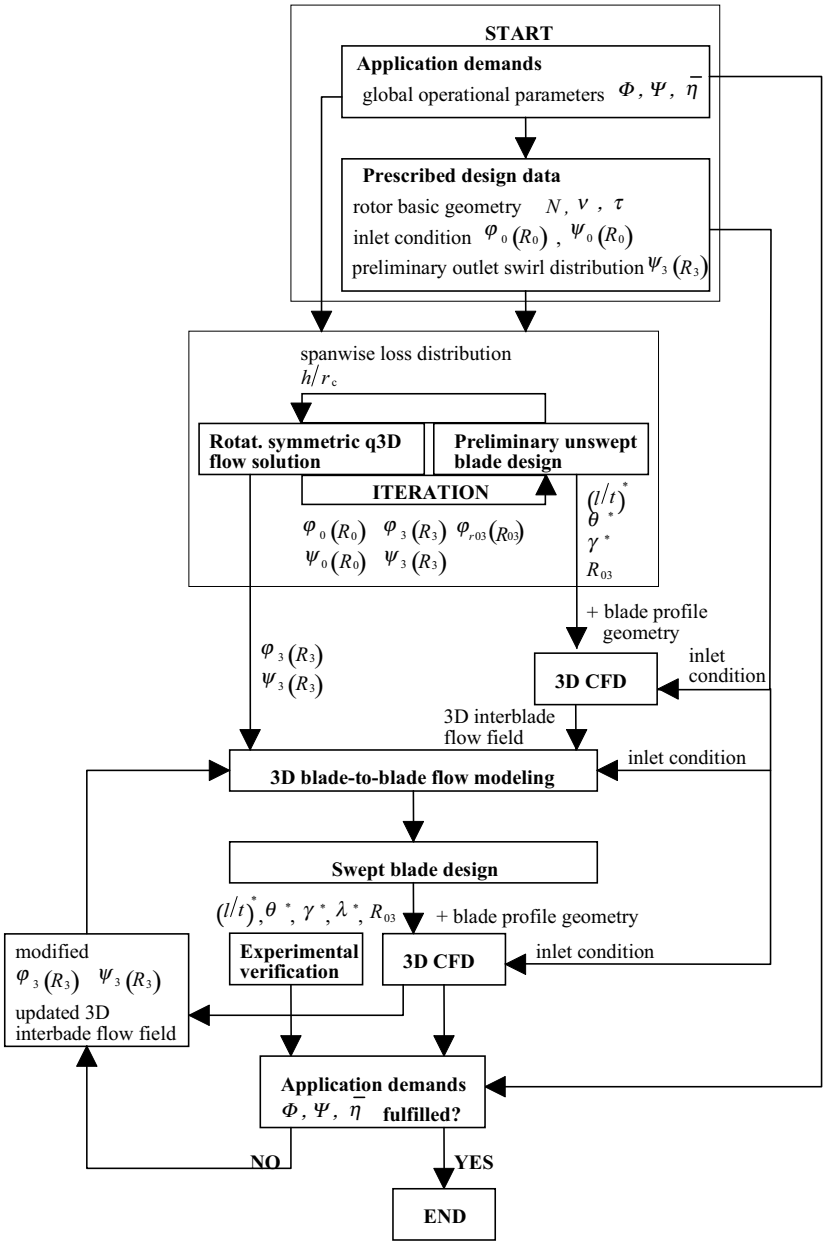

Fig. 1. Strategy for design of non-free vortex axial flow rotors with forward swept blades

4. Rotationally Symmetric Quasi-3D Flow Solution

In this section, derivation of quasi-3D rotationally symmetric theoretical rotor flow is discussed (see *Fig. 1*). At this preparatory design step, it is assumed that the flow develops through the NFV rotor fitting to conical stream surfaces. According to the assumption of a quasi-3D rotor flow field, all the descriptive relationships cited in this section regard pitchwise-averaged flow characteristics. With prescription of a spanwise constant blade circulation, the calculation method presented herein is a transition into a free vortex design methodology. *Fig. 2* shows the scheme of flow path through the rotor. Planes '0' and '3' are near upstream and downstream of the rotor, respectively.

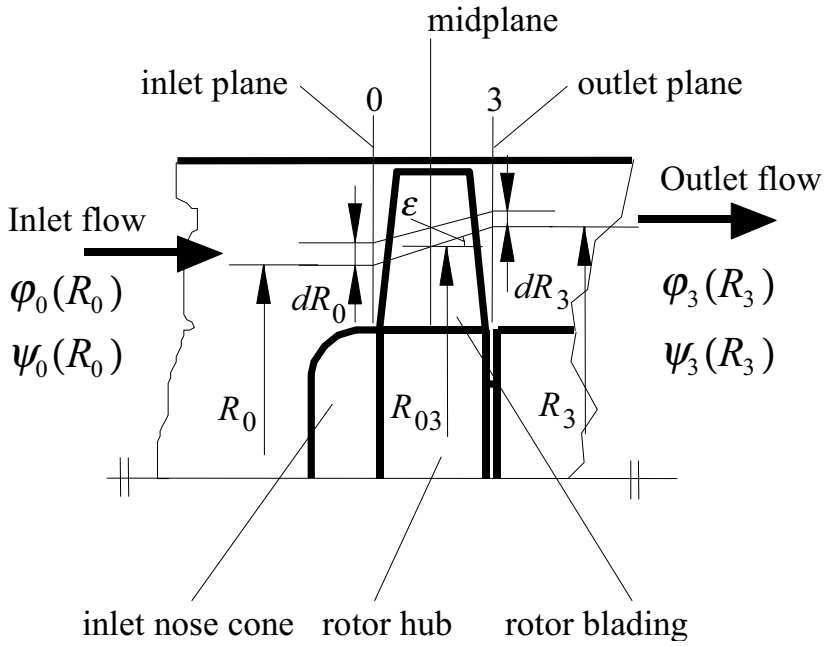

Fig. 2. Flow path through an isolated NFV rotor, representing an elemental conical cascade

In order to illustrate the computation methodology in a simple but lifelike manner, simplifying assumptions are considered, which are reasonable for fan rotors with no inlet guide vanes:

Incompressible flow through the rotor, $\rho = \text{constant}$,

Swirl-free inlet flow, $c_{0u} = 0$.

The calculation method allows an arbitrary axial inlet condition; i.e. c_{0x} may

vary with radius. Release of a uniform axial inlet condition is beneficial e.g. in the cases when a short rotor inlet nose cone is present, performing a streamline curvature effect and non-uniform inlet axial velocity profile. The c_{0x} distribution must be determined on the basis of measurements or auxiliary CFD studies (VAD et al. [25]).

Considering a conical stream surface fitting to radii r_0 and r_3 in the inlet and exit planes, the increase of total pressure performed by the rotor is expressed using the following equation:

$$p_{0t} + \Delta p_t = p_{3t}. \tag{1}$$

Eq. (1) can be expressed in a more detailed way considering that $\Delta p_t = \eta \Delta p_{\text{tid}} = \eta \rho u_3 c_{u3}$ with use of Euler equation of turbomachines, and $p_{3t} = p_3 + \rho c_3^2/2 = p_3 + (c_{3u}^2 + c_{3x}^2 + c_{3r}^2)\rho/2$. After introducing such details, let us make a derivative of *Eq.*(1) by r_3. It is assumed that p_{0t} is constant with radius. Furthermore, the Euler equation offers an approximation of $\partial p_3/\partial r_3 = \rho c_{3u}^2/r_3$. The flow downstream of plane 3 is assumed to be stabilised, i.e. the flow characteristics do not depend on the axial co-ordinate. As a consequence, the quasi-3D theoretical flow field characteristics depend only upon r_3 near downstream of the rotor, the spanwise derivative of *Eq.* (1) appears as an ordinary differential equation:

$$\frac{\mathrm{d}}{\mathrm{d}r_3}(\eta u_3 c_{u3}) = \frac{c_{u3}^2}{r_3} + \frac{1}{2}\frac{\mathrm{d}}{\mathrm{d}r_3}(c_{3u}^2 + c_{3x}^2 + c_{3r}^2). \tag{2a}$$

In dimensionless form:

$$\frac{1}{2}\frac{\mathrm{d}}{\mathrm{d}R_3}(\eta\psi_3) = \frac{1}{R_3}\left(\frac{\psi_3}{2R_3}\right)^2 + \frac{1}{2}\frac{\mathrm{d}}{\mathrm{d}R_3}\left[\left(\frac{\psi_3}{2R_3}\right)^2 + \varphi_3^2 + \varphi_{r3}^2\right]. \tag{2b}$$

The $\varphi_3(R_3)$ distribution must correspond to the prescribed global flow coefficient:

$$\Phi = \frac{2}{1-\nu^2}\int_\nu^1 \varphi_3 R_3 \,\mathrm{d}R_3. \tag{3}$$

Parameters of NFV $\psi_3(R_3)$ distribution are prescribed by the designer. Contrary to the former NFV design methods (e.g. BENCZE and SZLIVKA [3]; VAD and BENCZE [21]; BEILER and CAROLUS [2]), the presently proposed design method is not confined to swirl distributions prescribed with use of simple analytical functions. An arbitrary swirl distribution can be prescribed, harmonizing with the physical nature of rotor flow. The $\psi_3(R_3)$ and $\varphi_3(R_3)$ distributions must correspond to the prescribed global performance requirements:

$$\overline{\eta} \cdot \Psi \cdot \Phi = \frac{2}{1-\nu^2}\int_\nu^1 \eta\psi_3\varphi_3 R_3 \,\mathrm{d}R_3. \tag{4}$$

$\eta(R_3)$ can be approached if preliminary unswept blade geometry fitting to the rotationally symmetric theoretical flow field is calculated. Preliminary blade geometry

calculation is explained in Chapter 5. If the approximate geometry of elemental rotor blade cascades is computed, local losses related to the elemental cascades can be estimated considering profile losses and secondary losses. Tip clearance losses and annulus wall losses can also be estimated for the rotor and their distribution in the vicinity of the annulus walls must be suitably modelled, on the basis of design experiences. Eventually, a modelled spanwise loss and thus, efficiency distribution can be predicted. For preliminary blade design and estimation of losses, author refers to WALLIS [28].

It is also necessary to establish guidelines for estimation of $\varphi_3(R_3)$. R_3 and R_0 values related to the same hypothetical conical stream surface are calculated with numerical integration of the continuity equation, with knowledge of the inlet and outlet axial velocity profiles:

$$\int_v^{R_0} \varphi_0 R_0 \,\mathrm{d}R_0 = \int_v^{R_3} \varphi_3 R_3 \,\mathrm{d}R_3. \tag{5a}$$

The dimensionless maximum axial chord h/r_c of the blade must be estimated from preliminary unswept blade design (see Chapter 5). Its value can be refined in the consecutive iterative steps of determination of unswept cascade geometry. The axial chordwise-averaged radial velocity is approached as follows:

$$\varphi_{r03}(R_{03}) = \varphi_{03}(R_{03}) \cdot \tan\varepsilon, \tag{5b}$$

where

$$\varepsilon = \tan^{-1} \frac{R_3 - R_0}{h/r_c} \tag{5c}$$

is the cone half angle of the conical stream surface,

$$\varphi_{03} = \frac{\varphi_0(R_0) + \varphi_3(R_3)}{2} \tag{5d}$$

is the mean axial flow coefficient, and R_{03} is the mean radius of R_3 and R_0 (valid in the rotor midplane). Such computation must be carried out for several elemental rotors, establishing a $\varphi_{r03}(R_{03})$ distribution. According to the conical stream surface approach, an approximation of $\varphi_{r3}(R_3) = \varphi_{r03}(R_{03})(= \varphi_{r0}(R_0))$ is introduced.

With incorporation of system of *Eqs*. (2)–(5) and the estimation process of $\eta(R_3)$ into an iterative numerical solver procedure, outlet distributions of $\psi_3(R_3)$ and $\varphi_3(R_3)$ can be derived. Functions of $\varphi_0(R_0)$, $\varphi_3(R_3)$, $\varphi_{r03}(R_{03})$, and $\psi_3(R_3)$ form the basis of preliminary unswept blade design of an isolated rotor, as described in the next chapter. If the pre-swirl is non-zero due to the presence of a prerotator guide vane, there is no obstacle to consider the $\psi_0(R_0)$ function in the rotationally symmetric flow solution and also in preliminary unswept blade design. However, such case is not discussed herein for simplicity.

Flow characteristics for the test rotor are shown for three representative radii in *Table 1*. For the test rotor being discussed herein, $\varphi_0(R_0)$ has been specified in accordance with former experimental data, and $\psi_3(R_3)$ has been prescribed to

fit to the swirl distribution predicted by CFD for the unswept rotor in VAD et al. [24], so forming a basis for comparison. The swirl is nearly constant near the hub and increases progressively with radius, according to the non-free vortex design concept aiming an increased contribution of blade sections at higher radii to rotor performance. The nearly constant blade circulation in the vicinity of hub has been prescribed in order to moderate suction side blade root – hub corner stall, according to the proposition by VAD et al. [27]. $\varphi_3(R_3)$ and $\varphi_{r03}(R_{03})$ are computed. In order to consider the blockage effect of annulus wall boundary layers through the rotor – resulting in increased axial velocity in the dominant portion of span – the computational procedure has been carried out for a flow rate slightly higher than $\Phi = 0.50$. The reliability of this correction is based on experimental and CFD experiences.

Table 1. Design flow characteristics

	Hub	Midspan	Tip
R	0.676	0.838	1.000
φ_0	0.574	0.501	0.436
φ_3	0.501	0.519	0.540
φ_{r03}	0.000	0.028	0.000
ψ_3	0.600	0.645	0.808

5. Preliminary Unswept Blade Design

At this calculation phase, conical stream surfaces are assumed through the rotor (quasi-3D approach). The elemental blade cascades enclosed in two neighbouring conical stream surfaces can be developed into two-dimensional cascade planes (GRUBER [11]). Accordingly, the preliminary blade design can be based on a cascade approach. Given that the cone angle of the stream surfaces is relatively small, the distortion effect of transformation on the blade geometry is neglected herein.

There are many possibilities for utilisation of cascade approach. This paper presents a method based on experimental data on 2D stationary cascades (e.g. HOWELL [12]; CARTER and HUGHES [5], LIEBLEIN [16]). Such 'historical' 2D cascade data are applied widely even in these days in fan design (WALLIS [28]). The quasi-3D blade design presented in this paper gives a new utilisation area of these experimental data.

The following paragraph summarises the design methodology without a detailed presentation of all steps.

Fig. 2 presents a segment of the theoretical rotationally symmetric flow through an isolated rotor, enclosed in two neighbouring conical stream surfaces

of infinitely small radial distance. Let us consider an infinitely thin elemental rotor cascade enclosed in this stream tube. The radii of this stream tube at rotor inlet and outlet are R_0 and R_3, respectively. The thickness of the stream tube is $\mathrm{d}R_{03}$ in the rotor midplane and $\mathrm{d}R_3$ in the rotor outlet plane (*Fig. 2*).

The angular momentum equation must be applied to the fluid flowing in the conical stream tube, including the elemental rotor. It must be considered that the inlet flow is swirl-free. The angular momentum due to tangential friction forces developing on the conical stream surfaces is neglected. The axial component of angular momentum equation reads:

$$2\pi\rho c_{u3}c_{x3}r_3^2\,\mathrm{d}r_3 = \mathrm{d}M_x, \tag{6}$$

where $\mathrm{d}M_x$ is the momentum reacting on the elemental rotor by the flow. This momentum must be equal to the shaft torque driving the elemental rotor.

The mean flow angle inside the elemental rotor:

$$\beta_{03} = \cos^{-1}\frac{c_{x03}/\cos\varepsilon}{\sqrt{c_{x03}^2 + c_{r03}^2 + \left(u_{03} - \dfrac{c_{u3}}{2}\right)^2}} \tag{7}$$

where the denominator reads the mean relative velocity u_{03}. The shaft torque driving the elemental rotor is expressed as N times the elemental torque acting on a single elemental blade. The latter is calculated as the tangential forces acting on a single elemental blade (having a mean extension of $\mathrm{d}r_{03}\cos\varepsilon$ along the stacking line) multiplied by the arm of r_{03}. The shaft torque is:

$$\mathrm{d}M_x = Nr_{03}\left(\frac{\rho}{2}w_{03}^2\ell\mathrm{d}r_{03}\cos\varepsilon c_{\mathrm{lift}}\right)\frac{\sin(90^\circ - \beta_{03} + \delta)}{\cos\delta}, \tag{8}$$

where $\delta = \tan^{-1}(c_{\mathrm{drag}}/c_{\mathrm{lift}})$. In the following section, the blade pitch $t = 2r_{03}\pi/N$ is introduced. From continuity considerations, $c_{x03}r_{03}\mathrm{d}r_{03} = c_{x3}r_3\mathrm{d}r_3$ is applied. Using *Eq.* (7) $w_{03}\cos\beta_{03} = \frac{c_{x03}}{\cos\varepsilon}$ is derived. A combination of *Eqs.* (6) and (8), using the above relationships, followed by nondimensionalization results in the following equation:

$$\frac{\ell}{t}c_{\mathrm{lift}} = \frac{\psi_3}{R_{03}\varphi_{03}}\cdot\frac{\cos\varepsilon\cos\beta_{03}}{1 + \mathrm{tg}\,\delta\mathrm{tg}\,\beta_{03}}. \tag{9}$$

This is the so-called rotor work equation, derived here on a special way for quasi-3D flow approach. The next step is the determination of an optimum lift coefficient. For this purpose, the inlet and outlet flow angles must be calculated:

$$\beta_0 = \tan^{-1}\frac{R_0}{\varphi_{03}/\cos\varepsilon}, \tag{10a}$$

$$\beta_3 = \tan^{-1}\frac{R_3 - (\psi_3/2R_3)}{\varphi_{03}/\cos\varepsilon}. \tag{10b}$$

The optimum lift coefficient, as proposed e.g. by WALLIS [28], after HOWELL [12], on the basis of experimental data:

$$c^*_{\text{lift}} = 2\left(\frac{\cos\beta_0}{\cos\beta_3}\right)^{2.75}. \tag{11}$$

The optimum blade solidity $(\ell/t)^*$ can be calculated on the basis of *Eqs.* (9) and (11).

The optimum camber angle (central angle of circular arc blade chamber line) can be calculated e.g. with consideration of Carter's deviation angle rule (supplying an empirical relationship for the difference between the outlet flow angle and trailing edge blade angle, CARTER and HUGHES [5]):

$$\theta^* = \frac{\beta_0 - i^* - \beta_3}{1 - K\sqrt{1/(\ell/t)^*}}, \tag{12}$$

where the coefficient K is dependent upon the stagger angle γ (being calculated later) and thus, it must be determined in an iterative manner. The optimum incidence angle i^* (the difference between the inlet flow angle and leading edge blade angle) can be estimated on the basis of empirical formulae (e.g. LIEBLEIN [16]).

The optimum stagger angle – measured from the circumferential direction – is determined with use of the following relationship:

$$\gamma^* = 90^\circ - \left(\beta_0 - i^* - \frac{\theta^*}{2}\right). \tag{13}$$

The data sets of $(\ell/t)^*$, θ^* and γ^* for several elemental conical cascades enclosed in conical stream tubes of cone half-angles ε and mean radii R_{03} determine the preliminary optimum rotor blade skeleton geometry in an unswept blade approach. For an easier representation of blade geometry in CFD study in the consecutive step, the conical cascades are projected to cylindrical surfaces of mean radius equal to that of the conical surface. The geometry of blade profiles set on the camber lines is selected on the basis of design experiences or mechanical considerations.

From design point of view, the preliminary unswept blade geometry is necessary for estimation of spanwise loss distribution and $\varphi_{03}(R_{03})$, playing role in theoretical determination of the flow field, as described in Chapter 4. The preliminary unswept blade geometry forms the subject of CFD in a first approach of 3D blade-to-blade flow. The geometrical data of unswept blading serve also as a basis for lifelike comparison with swept blade geometry.

6. 3D CFD Technique

In order to obtain information on the 3D blade-to-blade flow, the preliminary unswept blade is subjected to a CFD investigation at the design flow rate (see *Fig.1*).

This CFD simulation must return accurately with the global design pressure rise coefficient. Furthermore, the CFD tool must resolve the viscous blade passage flow at a sufficient accuracy, including characteristic 3D rotor flow phenomena. A 3D turbulent finite element method is recommended. Although there exist theoretical means for inviscid flow calculation in swept cascades (e.g. YEH and SMITH [18]), consideration of viscosity effects is judged to be essential in axial flow rotor design.

Certain blade sections of a NFV rotor are of increased load, with an increased chance of blade boundary layer thickening. Hub corner stall and accumulation of low-energy fluid near the tip may also relate to a NFV behaviour. For an appropriate resolution of such effects, the use of a non-linear $\kappa - \varepsilon$ turbulence model is beneficial, as optional in code XENIOS of Department of Mechanics and Aeronautics, University of Rome 'La Sapienza'.

Considering the complex 3D blade passage flow developing in rotors of NFV operation, the accuracy of static pressure field measurements being carried out using a simple pressure measurement tool cannot be guaranteed. Such difficulties are to be surmounted with integration of a CFD tool in the design process. The appropriateness of the CFD device is proposed to be verified by 3D velocity measurement results, as reported in CORSINI et al. ([6], [7]).

During the design procedure, the CFD results are to be verified by global experiments (characteristic curve and efficiency measurements) once a version of rotor blading is manufactured.

7. 3D Blade-to-Blade Flow Modelling

At this phase (see *Fig. 1*), the relative streamlines in the vicinity of blade pressure side (PS) and suction side (SS) must be modelled. The 3D blade-to-blade flow is modelled the following way, as illustrated in *Fig. 3*:

A. It is assumed that the pitchwise-averaged flow data upstream and downstream of the rotor correspond to the $\varphi_0(R_0)$, $\varphi_3(R_3)$, and $\psi_3(R_3)$ distributions of the rotor flow field derived as described in Chapter 4.
B. It is assumed that the stream surfaces fit to conical surfaces near the blade. These conical surfaces represent inward flow near the PS (radial velocity component is directed toward the hub) and outward flow near the SS (radial velocity component is directed toward the tip). Such flow behavior is characteristic for rotors of non-free vortex operation (VAD and BENCZE [21]). The conicity distribution of the PS and SS cones $\varepsilon_{PS}(R_{03})$ and $\varepsilon_{SS}(R_{03})$ can be approximated using 3D CFD data obtained for the preliminary unswept rotor.

For a better view, characteristic quantities are indicated in *Fig. 3* for a streamline near the SS only. Quantities are defined for the PS flow in a similar manner.

The preliminary unswept rotor blading geometry (solidity, camber angle, stagger angle) calculated for the present test rotor does not differ significantly, especially

near and above midspan, from the unswept rotor studied formerly in CORSINI et al. [6] and VAD et al. [23], [24], [26]. Therefore, CFD data reported in these papers have been considered as a reliable basis for establishment of spanwise conicity distributions of the PS and SS cones in design of present test rotor.

It is expected on the basis of classical works (e.g. YEH and SMITH [18]) and recent communications (GLAS [9]) that blade sweep will change the 3D blade-to-blade flow and also the outlet axial flow coefficient and swirl distributions. Accordingly, corrections can be carried out on the $\varepsilon_{SS}(R_{03})$, $\varepsilon_{PS}(R_{03})$, $\varphi_3(R_3)$, and $\psi_3(R_3)$ distributions derived from the rotationally symmetric flow condition and preliminary unswept blade CFD, on the basis of CFD and design experiences. Such corrections are also optional after the CFD activity carried out for the first version of swept blade geometry.

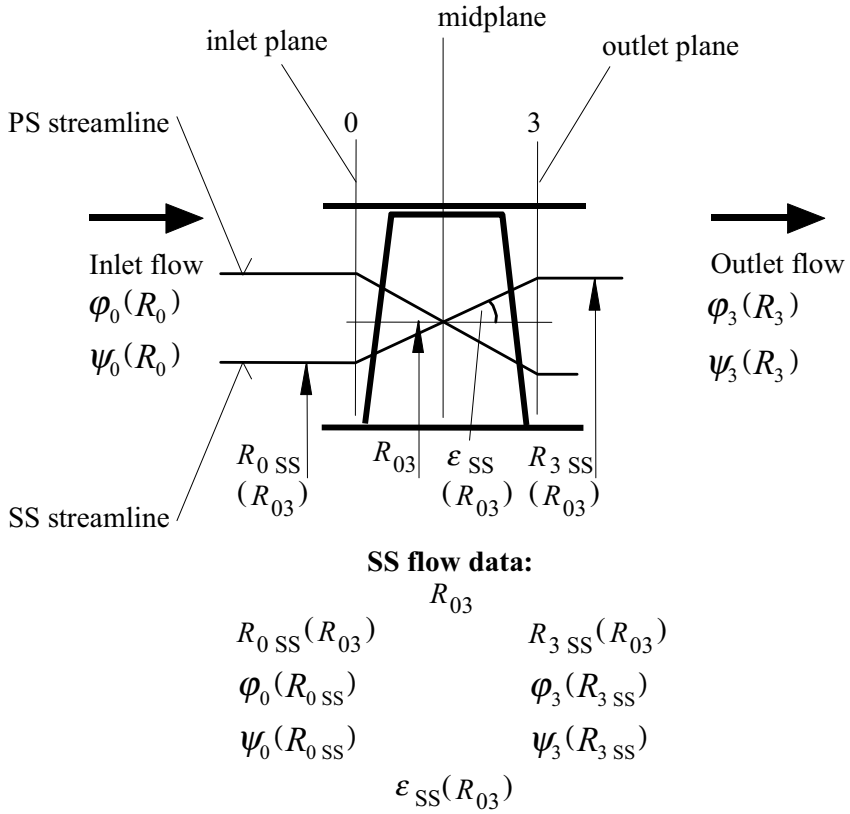

Fig. 3. 3D blade-to-blade flow model (quantities are indicated for the SS only, streamline inclinations are exaggerated)

8. Swept Blade Design

In the design method presented herein, the dihedral angle (e.g. SMITH and YEH [18]; and BEILER and CAROLUS [2]) is taken as zero.

As discussed in detail in VAD et al. [24], [26], the swept blade geometry is designed during a parallel optimisation of blade PS and SS. Let us consider a related couple of PS and SS cones of equal mean radius R_{03} (*Fig. 3*) onto which two streamlines passing near the blade at R_{03} fit. The equality of R_{03} for both PS and SS streamlines forms the basis of the proper optimisation. The streamlines are taken at the edge of the blade boundary layers, as in VAD et al. [24], [26]. In the following explanation, only the SS streamline is referred for simplicity.

The SS streamline enters the blade passage at the radius of R_{0SS} and exits at R_{3SS}. These radii can be estimated with use of conicity data $\varepsilon_{SS}(R_{03})$ derived from the CFD results (see Chapter 7), dimensionless mean axial chord h/r_c of preliminary unswept blading, and equation

$$\varepsilon_{SS} = \tan^{-1} \frac{R_{3SS} - R_{0SS}}{h/r_c} \tag{14a}$$

similar to *Eq.* (5c).

It is assumed that the local axial flow coefficients and swirl coefficients do not vary significantly in the pitchwise direction and thus, the inlet and outlet flow conditions near the SS can be suitably characterised by the data obtained from the rotationally symmetric flow solution (Chapter 4) $\varphi_0(R_{0SS})$, $\varphi_3(R_{3SS})$, $\psi_0(R_{0SS})$, and $\psi_3(R_{3SS})$. This assumption is reasonable, except for flow zones near the hub and casing walls where characteristic 3D flow phenomena occur (VAD and BENCZE [21]). The applicability of pitch-averaged data in the above-described approach has been confirmed in blade load computations by VAD et al. [24].

The radial velocity along the SS cone is calculated as

$$\varphi_{r3SS}(R_{3SS}) = \varphi_{r03SS}(R_{03}) = \varphi_{03SS}(R_{03}) \cdot \tan \varepsilon_{SS}(R_{03}), \tag{14b}$$

where

$$\varphi_{03SS} = \frac{\varphi_0(R_{0SS}) + \varphi_3(R_{3SS})}{2}, \tag{14c}$$

similarly to *Eqs.* (5b) and (5d).

Based on the above, the flow on the SS is considered as a flow through a conical blade cascade of $\varepsilon_{SS}(R_{03})$. Using data $\varphi_0(R_{0SS})$, $\varphi_3(R_{3SS})$, $\psi_0(R_{0SS})$, $\psi_3(R_{3SS})$, and $\varphi_{r03SS}(R_{03})$, optimum cascade geometrical data $(\ell/t)^*_{SS}(R_{03})$, $\theta^*_{SS}(R_{03})$ and $\gamma^*_{SS}(R_{03})$ can be determined separately for the SS, exactly the same way as described for the preliminary unswept blade design in Chapter 5.

Following the same train of thoughts, using the data of $\varepsilon_{PS}(R_{03})$ established from CFD results, optimum cascade geometrical data $(\ell/t)^*_{PS}(R_{03})$, $\theta^*_{PS}(R_{03})$ and $\gamma^*_{PS}(R_{03})$ can be determined separately also for the PS on the same mean radius R_{03}.

Carrying out such two-side optimisation for several mean radii R_{03}, two versions of blade camber geometry are derived, representing optimum blade shapes

separately for the SS and PS flow circumstances. The swept blade geometry must unify these parallel shape demands, thus performing an accommodation of 3D blade-to-blade flow.

Given that the flow condition differs significantly on the SS and PS due to the difference in inclination of SS and PS streamlines, it is obvious that the SS and PS optimum shape may show considerable differences. The conical cascades of optimised geometry on both SS and PS must be projected to cylindrical surfaces of mean radius R_{03} equal to that of the conical surface. The experience shows that the optimum camber and stagger angles (projected to the cylindrical surfaces) do not differ significantly for the SS and PS. As a reasonable compromise, averaging the SS and PS optimum angles derives the swept blade camber and stagger angles:

$$\theta^*_{\mathrm{SW}}(R_{03}) = \frac{[\theta^*_{SS}(R_{03}) + \theta^*_{\mathrm{PS}}(R_{03})]}{2}, \tag{15}$$

$$\gamma^*_{\mathrm{SW}}(R_{03}) = \frac{[\gamma^*_{SS}(R_{03}) + \gamma^*_{\mathrm{PS}}(R_{03})]}{2}. \tag{16}$$

In spite of above, a significant difference appears in the SS and PS blade solidities (more times ten percent for present test rotor). According to the NFV swirl distribution and the nature of axial velocity profiles, it can be generally stated that $(\ell/t)^*_{\mathrm{PS}}(R_{03}) > (\ell/t)^*_{\mathrm{SS}}(R_{03})$. Such contradictory conditions can be simultaneously fulfilled exclusively with sweeping the blades forward to an appropriate extent.

Instead of presenting geometrical relationships, the sweep calculation is illustrated in *Fig. 4*. The classical definition of blade sweep generally used in the turbomachinery society (e.g. SMITH and YEH [18]; BEILER and CAROLUS [2]) has been applied in this paper.

Before explanation of sweep calculation, the sweep is defined in a lifelike way. The blade sweep can be obtained in a recursive manner, dividing the blading to several elemental rotors fitting to cylindrical surfaces. The circular arc camber line at a given radius R_{03i} (with stagger) must be drawn, and the halving point P_i of the blade chord must be marked. A radial line fitting to this halving point must be assumed. The halving point P_{i+1} of the chord at the consecutive radius R_{03i+1} must be stacked to this radial line. The next camber line (with stagger) must be drawn in this position. Then, the camber line at R_{03i+1} must be 'swept forward' by translating the camber line parallel to the chord in the upstream direction. During translation, P_{i+1} is forwarded to point P'_{i+1} at the radius R_{03i+1}. Angle $P_{i+1}P_iP'_{i+1}$ is the sweep angle λ. According to the sign convention used in the turbomachinery society (e.g. SMITH and YEH [18]; BEILER and CAROLUS [2]), λ has a negative value for forward sweep.

As *Fig. 4* shows, the optimum sweep angle $\lambda^*(R_{03})$ for the mean radius R_{03} can be obtained as follows. The SS and PS optimum conical chords characterized by $\varepsilon_{\mathrm{SS}}(R_{03})$, $(\ell/t)^*_{\mathrm{SS}}(R_{03})$, $\varepsilon_{\mathrm{PS}}(R_{03})$, and $(\ell/t)^*_{\mathrm{PS}}(R_{03})$ are represented as lines intersected at radius R_{03}. The conical chords fit to identical plane at a given mean radius R_{03}. Such plane is determined by the radial direction (no dihedral prescribed) and $\gamma^*_{\mathrm{SW}}(R_{03})$. The conical chords form the diagonals of a parallelogram. The angle

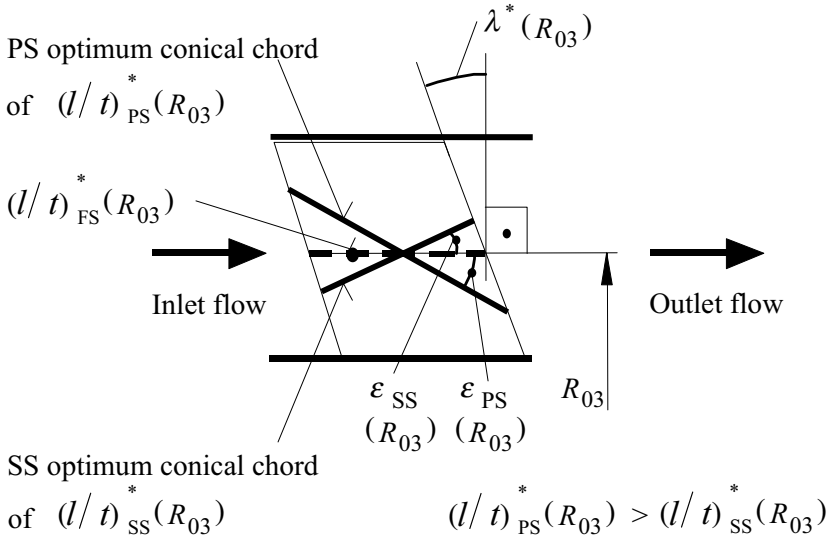

Fig. 4. Explanation of optimum blade sweep angle calculation. (The image of the blade and the represented quantities are projected to the radial plane in the figure. Conical chord inclinations are exaggerated.)

between the radial direction and the leading (or trailing) edge of the parallelogram is considered as the optimum sweep angle $\lambda^*(R_{03})$. The length of chordwise parallelogram side(s) (appearing as a projection to the cylindrical surface of R_{03}) is considered as an optimum chord length $(\ell/t)^*_{SW}(R_{03})$.

The blading having optimum sweep calculated for several R_{03} radii encloses approximately the optimum conical chords for both SS and PS. Therefore, it accommodates the realistic 3D blade-to- blade flow developing in the NFV rotor. If the computed optimum sweep angle does not vary considerably with radius, it is proposed to set it to a spanwise constant representative value.

According to the nature of swept blade design method presented herein, the optimum solidity, camber angle and stagger angle values obtained for the swept rotor are usually higher than those computed for the preliminary unswept blading.

9. Completion of Design Method

The swept bladed rotor must be subjected to a parallel CFD study and global experiments (*Fig. 1*). If the characteristic curve and efficiency measurements verify that the prescribed operational demands are fulfilled with a reasonably low relative difference, the design procedure is considered to be completed. Otherwise, the outlet flow data and the 3D interblade flow model must be modified on the basis of

CFD results, which have been verified by the global experiments. The 3D blade-to-blade flow modelling and swept blade design must be repeated on the basis of the modified data. Such procedure is optional to be repeated in an iterative manner, according to the demands (*Fig. 1*).

The blade geometry can also be optionally refined on the basis of CFD studies, independently from the entire design procedure. For example, a need for modification of blade shape near the leading edge for tuning the flow incidence angle can be established from the CFD data in a lifelike manner.

The design methodology can be extended to design of guide vanes with blade sweep.

10. Design Example

Table 2 presents a comparison between geometrical data determined for the preliminary unswept rotor and the first version of swept rotor (conf. Chapter 2) on the basis of design methodology summarised above. The geometrical data are documented for three representative radii. The data are considered as characteristics of blade sections projected to cylindrical surfaces of R.

It is conspicuous that blade solidity, camber angle, and stagger angle are increased for the swept rotor, especially below and near midspan. This tendency is expected to correspond to the fact that blade sweep results in decreased blade lift (e.g. SMITH and YEH [18]) and thus, the solidity, camber angle and stagger angle must be increased for retaining rotor performance.

The swept model rotor presented herein forms the basis of further CFD study (CORSINI et al. [7]), in accordance with the design strategy outlined in *Fig. 1*.

Table 2. Comparative data of blade geometry for the unswept and swept rotors

		Hub	Midspan	Tip
	R	0.676	0.838	1.000
Unswept rotor	$(\ell/t)^*$	1.74	1.15	1.13
	θ^*	34.4°	22.7°	20.3°
	γ^*	55.3°	43.0°	37.4°
	λ	0°	0°	0°
Swept rotor	$(\ell/t)^*$	1.79	1.23	1.13
	θ^*	35.4°	25.4°	20.3°
	γ^*	56.2°	43.1°	37.4°
	λ	−35°	−35°	−35°

11. Summary

A novel design strategy for high-performance non-free vortex axial flow rotors with forward swept blades has been presented herein. The design methodology incorporates the determination of an optimum extent of forward blade sweep, ensuring an appropriate accommodation of 3D blade-to-blade flow by the blade geometry. The design strategy involves theoretical considerations for computation of a quasi-3D rotationally symmetric flow through the rotor, cascade concept for preliminary unswept blade design, CFD activity for modelling the 3D blade-to-blade flow, a concerted optimisation of suction side and pressure side blade geometry based on cascade concept, and determination of optimum blade sweep guaranteeing a simultaneous fulfilment of optimum geometrical demands on both suction side and pressure side. The computer-aided rotor optimisation strategy is built up in an iterative manner, also including experimental verification of rotor design.

Acknowledgement

The author acknowledges the support of OTKA (Hungarian National Foundation for Science and Research) under contract T 025361, the Hungarian Ministry for Education under contract FKFP 0356/1999, the Hungarian Academy of Sciences by a János Bolyai Hungarian National Research Grant, Ref. No. BO/00150/98, Hungarian-Italian Bilateral S&T Project I-28/98, and Hungarian-Austrian Bilateral S&T Project A-34/98.

Nomenclature

c	[m/s]	absolute velocity
c_{drag}	[–]	drag coefficient
c_{lift}	[–]	lift coefficient
h	[m]	mean axial chord
i	[deg]	incidence angle (measured positive from the inlet blade angle if results in increased lift)
ℓ	[m]	blade chord
M	[Nm]	torque
N	[–]	blade number
p	[Pa]	pressure
Δp	[Pa]	pressure rise
r	[m]	radius
$R = r/r_c$	[–]	dimensionless radius
$t = 2r\pi/N$	[m]	blade pitch
u	[m/s]	circumferential velocity ($r \cdot \omega$)
u_c	[m/s]	reference velocity ($r_c \cdot \omega$)
w	[m/s]	relative velocity

β	[deg]	flow angle (measured from the axial direction)
γ	[deg]	blade stagger angle (measured from the circumferential direction)
δ	[deg]	$\tan^{-1}$ of drag-to-lift ratio
ε	[deg]	cone half angle of conical stream surface
θ	[deg]	camber angle
λ	[deg]	blade sweep angle (measured as described in Chapter 8)
Φ	[–]	design global flow coefficient (area-averaged axial velocity in the annulus divided by u_c)
Ψ	[–]	design global ideal total pressure rise coefficient (mass-averaged ideal total pressure rise in the annulus normalised by $\rho u_c^2/2$)
$\varphi = c_x/u_c$	[–]	local pitchwise-averaged axial flow coefficient
$\varphi_r = c_r/u_c$	[–]	local pitchwise-averaged radial flow coefficient
$\psi = 2Rc_u/u_c$	[–]	local pitchwise-averaged swirl coefficient
ρ	[kg/m^3]	air density
ν	[–]	hub-to-casing diameter ratio
τ	[m]	average tip clearance
ω	[1/s]	rotor angular speed
η	[–]	local efficiency (ratio of realised and ideal local total pressure rise)
$\overline{\eta}$	[–]	mean efficiency (ratio of realised and ideal averaged total pressure rise)

Subscripts and Superscripts

c	casing wall
id	ideal (total pressure rise)
PS, SS	pressure side, suction side
r, u, x	radial, tangential, axial
SW	swept blade
t	total (pressure)
0	rotor inlet plane
3	rotor exit plane
03	rotor midplane, mean value inside the rotor
$*$	optimum value

References

[1] BEILER, M. G., Untersuchung der dreidimensionalen Strömung durch Axialventilatoren mit gekrümmten Schaufeln, Doctoral Thesis, VDI Fortschrittberichte, Reihe 7 (Strömungstechnik), Nr. 298. VDI Verlag GmbH, Düsseldorf, Germany, 1996.

[2] BEILER, M.G. – CAROLUS, T. H., Computation and Measurement of the Flow in Axial Flow Fans with Skewed Blades, *ASME Journal of Turbomachinery*, **121** (1999), pp. 59–66.

[3] BENCZE, F. – SZLIVKA, F., A New Method for the Design of Axial Flow Fans of Changing Circulation, *Proceedings of the 8th Conference on Fluid Machinery*, 1987, Budapest, Hungary, pp. 94–102.

[4] BREUGELMANS, F. A. E., Energy Efficient Design Through Fluid Dynamics Improvements in Turbocomponents, *International Seminar on Thermal and Fluid Engineering for Advanced Energy Systems*. Institute of Advanced Material Study, Kyushu University, Kasuga, Japan, July 23–24 1997. (lecture note, Von Karman Institute for Fluid Dynamics).

[5] CARTER, A. D. S. – HUGHES, H. P., A Theoretical Investigation into the Effect of Profile Shape on the Performance of Aerofoils in Cascade, R. & M. 2384, British ARC, 1946.

[6] CORSINI, A. – RISPOLI, F. – BENCZE, F. – VAD, J., Concerted Experimental and Numerical Studies on Axial Flow Fan Rotor Aerodynamics, IMechE paper C557/106/99, *Proc. 3rd European Conference on Turbomachinery Fluid Dynamics and Thermodynamics*, London, United Kingdom, 1999, pp. 519–531.

[7] CORSINI, A. – RISPOLI, F. – BENCZE, F. – VAD, J., Effect of Blade Sweep in a High Performance Axial Flow Rotor, accepted for *4th European Conference on Turbomachinery Fluid Dynamics and Thermodynamics*, 2001, Florence, Italy.

[8] GLAS, W. – KUHN, K., Vergleich der Festigkeit von gepfeilten und ungepfeilten Schaufeln in axialen hydraulischen Turbomaschinen, Beitragstexte (V17 bis V39) zum *XXX. Kraftwerkstechnischen Kolloquium*, pp. 110–119, October 1998, Dresden, Germany.

[9] GLAS, W., private communication. Technical University of Graz, Institute for Hydraulic Fluid Machinery, Graz, Austria, 2000.

[10] GLAS, W., Optimierung gepfeilter Pumpenschaufeln mit Evolutionären Algorithmen, Ph.D. Thesis, Technical University of Graz, Institute for Hydraulic Fluid Machinery, Graz, Austria, 2000.

[11] GRUBER, J. (leading author), *Ventilátorok*, Műszaki Könyvkiadó, Budapest, 1978, 4th edition (in Hungarian).

[12] HOWELL, A. R., The Present Basis of Axial Flow Compressor Design, Part I: Aeronautical Research Council R. and M. 2095, London; Part II: R. A. E. Report E 3961, 1942.

[13] KODAMA, H. – NAMBA, M., Lifting Surface Theory for Steady Aerodynamic Analysis of Ducted Counter Rotation Propfan, *ASME Paper No. 92-GT-14*, 1992.

[14] KUHN, K., Experimentelle Untersuchung einer Axialpumpe und Rohrturbine mit gepfeilten Schaufeln, Ph.D. Thesis, Technical University of Graz, Institute for Hydraulic Fluid Machinery, Graz, Austria, 2000.

[15] LAKSHMINARAYANA, B., *Fluid Dynamics and Heat Transfer of Turbomachinery*, John Wiley & Sons, Inc., 1996.

[16] LIEBLEIN, S., Experimental Flow in Two-Dimensional Cascades, Chapter VI in: Members of the staff of Lewis Research Center: *Aerodynamic Design of Axial-Flow Compressors*. NASA SP-36, Washington D. C., 1965.

[17] MOHAMMED, K. P. – RAJ, D. P., Investigations on Axial Flow Fan Impellers With Forward Swept Blades, *ASME Journal of Fluids Engineering*, September 1977, pp. 543–547.

[18] SMITH, L. M. – YEH, H., Sweep and Dihedral Effects in Axial-Flow Turbomachinery, *ASME Journal of Basic Engineering*, **85** (1963), pp. 401–416.

[19] SRIVASTAVA, R. – MEHMED, O., On the Static Stability of Forward Swept Propfans, *AIAA paper No. 93-1634-CP.*, 1993.

[20] THOMSON,D. – WATSON, K. – NORDEN, C. – GORRELL, S. – BRAISTED, W. – BROCKMAN, R., Assessment of Organic Matrix Components for a Forward Swept Fan Stage, *AIAA Paper No. 94-1353-CP.*, 1994.

[21] VAD, J. – BENCZE, F., Three-Dimensional Flow in Axial Flow Fans of Non-Free Vortex Design, *International Journal of Heat and Fluid Flow*, **19**, December 1998, pp. 601–607.
[22] VAD, J. – BENCZE, F., Experimental Guidelines for Retaining Energy-Efficient Axial Flow Rotor Cascade Operation Under Off-Design Circumstances, *Proceedings of 4th International Symposium on Engineering Turbulence Modeling and Experiments*, May 1999, Corsica, France, pp. 751–760. (published in: '*Engineering Turbulence Modeling and Experiments*', Elsevier, 1999).
[23] VAD, J. – BENCZE, F. – CORSINI, A. – RISPOLI, F., Three-Dimensional Flow Development Inside an Axial Flow Fan of Non-Free Vortex Design, *Proceedings of 11th Conference on Fluid and Heat Machinery and Equipment*, September 1999, Budapest, Hungary (CD-ROM material).
[24] VAD, J. – BENCZE, F. – CORSINI, A. – RISPOLI, F., Non-Free Vortex Flow Effects in an Axial Flow Rotor, *Periodica Polytechnica, Mechanical Engineering Series*. A Contribution to International Technical Sciences, published by the Budapest University of Technology and Economics, Budapest, Hungary. (accepted for publication in 1999).
[25] VAD, J. – CSONKA, SZ. – BENCZE, F., Experimental and Numerical Investigation of Axial Flow Rotor Inlet Condition, *Proceedings of MICROCAD*' 99 Conference, February 1999, Miskolc, Hungary, pp. 175–180.
[26] VAD, J. – BENCZE, F. – CORSINI, A. – RISPOLI, F., Design Aspects of Three-Dimensional Flow in High Performance Axial Flow Ventilating Fans, *Proceedings of 6th International Symposium on Ventilation for Contaminant Control (VENTILATION'2000)*, June 2000, Helsinki, Finland, pp. 108–110.
[27] VAD, J. – BENCZE, F. – GLAS, W. – JABERG, H., Comparative Investigation on Axial Flow Pump Rotors of Free Vortex and Non-Free Vortex Design, *Periodica Polytechnica, Mechanical Engineering Series*. A Contribution to International Technical Sciences, published by the Budapest University of Technology and Economics, Budapest, Hungary. (accepted for publication in 2000).
[28] WALLIS, R. A., *Axial Flow Fans and Ducts*, John Wiley & Sons, New York, 1983.
[29] WENNERSTROM, A. J. – PUTERBAUGH, S. L., A Three Dimensional Model for the Prediction of Shock Losses in Compressor Blade Rows, *ASME Journal of Engineering for Gas Turbines and Power*, **106** (1984), pp. 295–299.
[30] WRIGHT, T. – SIMMONS, W. E., Blade Sweep for Low-Speed Axial Fans, *ASME Journal of Turbomachinery*, **112**, January 1990, pp. 151–158.
[31] YAMAGUCHI, N. – TOMINAGA, T. – HATTORI, S. – MITSUHASHI, T., Secondary-Loss Reduction by Forward-Skewing of Axial Compressor Rotor Blading, *Proc. Yokohama International Gas Turbine Congress*, (1991), pp. II.61–II.68.